

COLLECTIVE EFFECTS AND THEIR CONTROL AT THE SPALLATION NEUTRON SOURCE RING*

J. Wei[†], M. Blaskiewicz, J. Brodowski, P. Cameron, D. Davino, A. Fedotov, H. Hahn
H. Hseuh, Y.Y. Lee, D. Raparia, S.Y. Zhang, BNL; V. Danilov, S. Henderson, J. Holmes
J.G. Wang, ORNL; M. Furman, M. Pivi, LBNL; S. Kurennoy, R. Macek, LANL, USA

Abstract

One of the primary tasks in the design of the Spallation Neutron Source (SNS) ring is to control collective effects including space charge, transverse and longitudinal instabilities, and electron cloud. Transverse painting is used to alleviate space charge force; longitudinal painting along with chromatic sextupoles are used to enhance Landau damping; injection kicker vacuum pipes are carefully shielded, and extraction kicker impedances are measured in detail and optimized; beam halo, beam loss and electron production are minimized; finally, damping systems at various frequencies are planned. This paper summarizes these design implementations.

1 COLLECTIVE PHENOMENA

The SNS ring is designed to accumulate up to 2×10^{14} protons of 1 GeV kinetic energy at a repetition rate of 60 Hz [1]. Dominant collective effects include space charge and halo generation, impedance-driven instabilities, impedance-induced closed-orbit deviation and heating, and electron cloud.

1.1 Space-charge & Beam Halo

Space charge is a fundamental limitation in high-intensity rings. Transversely, the spread of tune shift may cause resonance crossing and beam-halo generation (Fig. 1). For a bunch of N_0 particles with bunching factor B_f , the incoherent tune shift is given by

$$\Delta\nu_{x,y} = -\frac{f_{sc}N_0r_0R_0}{2\pi B_f\nu_{x,y,0}\beta^2\gamma} \left[\frac{\gamma^{-2} - \eta_e}{\sigma_{x,y}(\sigma_x + \sigma_y)} + A_{im}^e(\gamma^{-2} - \eta_e) + A_{im}^m \right] \quad (1)$$

where r_0 is the classical radius of proton, R_0 is the average radius of circumference, $\nu_{x,y,0}$ and $\sigma_{x,y}$ are the base transverse tunes and rms beam sizes, and f_{sc} (1/2 for an uniform, 1 for a Gaussian distribution) is the form factor, and η_e is the neutralization factor. The contribution from the electric and magnetic images of the beam are represented by A_{im}^e and A_{im}^m , respectively. Note that collective response must be considered for resonance-crossing analysis [2]. Longitudinally, space charge produces a defocusing potential below transition (γ_T)

$$V_{sc} = -\hat{I}Z_{||}; \quad Z_{||} = -j\frac{nZ_0g_0}{2\beta\gamma^2}; \quad g_0 = 1 + 2\ln\frac{2b}{w+h} \quad (2)$$

where the peak current $\hat{I} \approx 100$ A, $n = \omega/\omega_0$ is the frequency harmonic, $Z_0 \approx 377\Omega$, w and h are half width and height of the beam, and b is the half beam-pipe radius [3].

* Work performed under the auspices of the US Department of Energy.

[†] jwei@bnl.gov

Table 1: Estimated coupling impedance at frequency below 10 MHz. The revolution frequency, $\omega_0/2\pi$, is 1.058 MHz.

Mechanism	$Z_{ }/n [\Omega]$	$Z_{\perp} [k\Omega/m]$
Space charge	$-j196$	$j(-5.8 + 0.45) \times 10^3$
Ext. kicker	$0.6n + j50$	$74 + j209$
Inj. kicker & pipe	$0.17/n$	12 at 200 kHz
Inj. foil assembly	$j0.05$	$j4.5$
Resistive wall	$(j+1)0.71$	$(j+1)8.5$ at ω_0
B.b. BPM	$j3.0$	$j15$
B.b. bellows	$j1.3$	$j11$
B.b. Steps	$j1.9$	$j16$
B.b. ports	$j0.49$	$j4.4$
B.b. Valves	$j0.15$	$j1.4$
B.b. Collimator	$j0.22$	$j2.0$

1.2 Impedance-driven Instabilities

As listed in Table 1, the leading impedance source contributing to possible instability is due to the extraction kicker modules located inside the beam vacuum pipe.

Table 2 lists the estimated threshold at which the corresponding effects become significant for a 2 MW beam. Four-family chromatic sextupoles are used to either damp instabilities or avoid resonance crossing without compromising the dynamic aperture [4].

1.3 Impedance-related Effects

The circulating beam deviates from the center of extraction kickers by up to 4.5 cm. The transverse coupling impedance introduces an intensity-dependent deflection

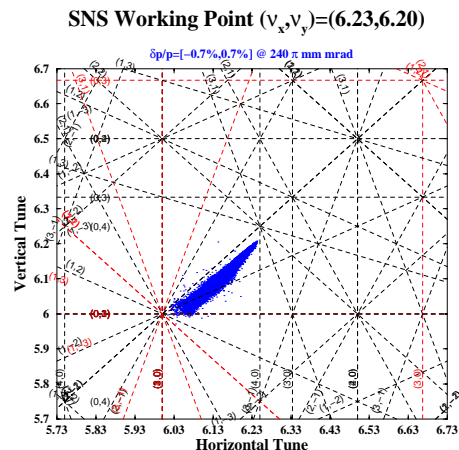


Figure 1: Tune spread of a 2 MW proton beam in the SNS ring. Structure resonances are indicated in red.

Table 2: Collective effects and estimated thresholds for the SNS accumulator ring. Space charge effects are treated separately (Sections 1.1 and 2.4).

Mechanism	Threshold	Comments
Trans. space charge	$\Delta\nu_{sc} \sim -0.2$	resonance cross
Long. space charge	60 kV RF voltage	15 kV induced volt.
Long. microwave	$ Z_{\parallel}/n = 32 \Omega$	Keil-Schnell crit.
Trans. microwave ($\xi = 0$)	$ Z_{\perp} = 1.3 \text{ k}\Omega/\text{m}$ (resistive wall)	at 200 kHz rise time $> 300 \mu\text{s}$
Trans. microwave ($\xi = -3$)	$ Z_{\perp} = 100 \text{ k}\Omega/\text{m}$ (resistive wall)	at 200 kHz
Trans. microwave ($\xi = 0 \sim -3$)	$ Z_{\perp} \approx 60 \text{ k}\Omega/\text{m}$ (extraction kicker)	at $\sim 10 \text{ MHz}$ w/o space charge
Trans. microwave ($\xi = 0 \sim -3$)	$ Z_{\perp} \approx 300 \text{ k}\Omega/\text{m}$ (extraction kicker)	at $\sim 50 \text{ MHz}$ w/o space charge

that produces a closed-orbit deviation with peak amplitudes varying from the center to the edge of the beam pulse (Fig. 2). Damping of such a “banana-closed orbit” requires a fast ($\sim 100 \text{ ns}$) feedback system.

For a fixed-energy ring, the eddy-current causes heating complications only in the injection ($\tau_{rise} \approx 200 \mu\text{s}$) and extraction ($\tau_{rise} \approx 200 \text{ ns}$) regions.

1.4 Electron-cloud Effects

Electron-cloud is a potential threat to high-intensity operation. Main sources of low-energy (tens of eV) electrons are the injection stripping foil and surface backscattering, proton grazing loss at collimator surface, single-bunch multipacting (Fig. 3), and gas ionization (see Section 2.3) [5]. The effects include neutralization tune shift (Eq. 1) and resonance crossing, and electron-cloud instabilities.

2 IMPEDANCE MINIMIZATION

Instability growth is primarily associated with the resistive part of the impedance. The leading source is from the extraction kicker modules located inside the vacuum pipe.

2.1 Extraction Kicker & Power Supply

Copper sheets are placed inside the ferrite core as flux breaks to reduce the ferrite loss and longitudinal impedance. Transverse coupling-impedance reduction of the 14 kickers is realized with the design of the pulse-forming network (PFN) circuits with low termination

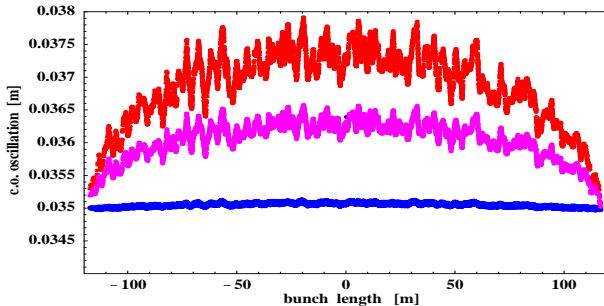


Figure 2: Orbit deviation for 3 turns due to beam-centroid offset from the mechanical center of the extraction kickers.

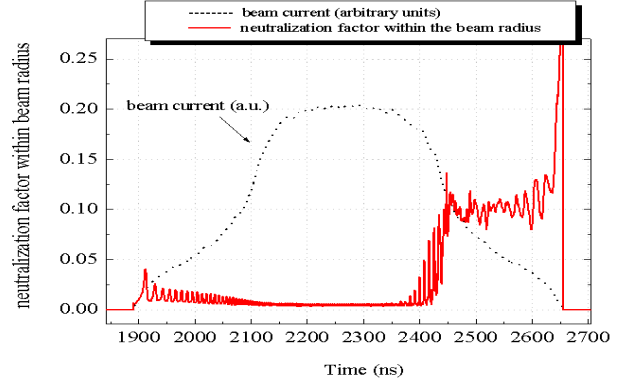


Figure 3: Simulation of single-bunch electron multipacting with a peak secondary-emission yield of 2.

impedance (25Ω). The measured transverse impedance is well presented by a resonator-equivalent circuit

$$Z_{\perp}^{kk} = \frac{c}{\omega h^2} \left[\left(\frac{1}{R} + \frac{1}{j\omega L} + j\omega C \right)^{-1} + j\omega L_s \right] \quad (3)$$

where $R = 23.89 \Omega$ is the external damping resistor in parallel of ferrite losses, $L = 0.936 \mu\text{H}$ is the inductance measured externally at the bus bar, $C = 21.7 \text{ pF}$ is the feed thru plus stray capacitance associated with the bus bar, and $L_s = 0.798 \mu\text{H}$ is the inductance on beam side with open bus bar [6]. Efforts are made to maximize the height of the vertical kickers without excessive increase of driving current and voltage. The lumped Blumlein PFNs are placed outside of ring tunnel for easier maintenance. It is experimentally verified that ferrite material of relatively low permeability and low resistive-loss is beneficial only if the PFN is not terminated with a low impedance (Fig. 4).

2.2 Resistive Wall & Ceramic-pipe Coating

Except for the injection kicker and some beam-diagnostics sections, stainless-steel vacuum pipe is used. The coupling impedance is noticeable only for low frequencies (lowest betatron sideband 200 kHz)

$$Z_{\parallel}^{rw} = n(1+j) \frac{\beta Z_0 d_s}{2b}; \quad Z_{\perp}^{rw} = \frac{2R_0}{\beta b^2} \frac{Z_{\parallel}^{rw}}{n}; \quad d_s = \sqrt{\frac{2\rho_r}{\mu_0 \omega}} \quad (4)$$

where μ_0 is the permeability, ρ_r is the resistivity, d_s is the skin depth, and b is the pipe radius. A large contribution is from the small-aperture collimators.

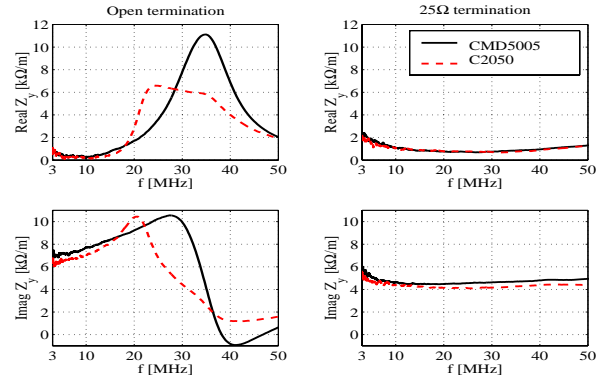


Figure 4: Comparison of bench-measured coupling impedance for open and 25Ω PFN termination, and high (1600) and medium (100) permeability ferrite.

Ceramic vacuum pipes are used to avoid eddy-current heating corresponding to an injection-bump risetime of about 200 μ s. Their coupling impedance is reduced by an internal, 1 μ m copper-film coating (much thinner than the skin depth $d_s \approx 0.9$ mm). Longitudinally, the metal coating acts like a pure resistive conductor. Denote the metal coating and the ceramic with subscripts m and c , respectively. When the permeability of the kicker ferrite is much larger than 1, the impedances are given by [7]

$$Z_{\parallel}^{ct} \approx \frac{L_c \rho_{r,m}}{2\pi b d_m}; \quad Z_{\perp}^{ct} \approx \frac{j L_c Z_0}{\pi b^2} \frac{-1}{1 - j\omega \mu_0 b d_m \rho_{r,m}^{-1}} \quad (5)$$

where L_c is the section length and $d_{m,c}$ are the thickness. At low frequencies (below 100 kHz) where d_s^2 exceeds the product of the chamber's radius b times the layer's thickness d_m , the transverse impedance rapidly goes to zero. A second, 0.1 μ m thin TiN coating is applied to suppress the secondary yield of electron generation. A dc bypass is also provided via external enclosure of the kicker magnets.

2.3 Electron Cloud

Effective impedance of an electron cloud is proportional to the neutralization [8]

$$Z_{\perp}^{ep} \approx \frac{\eta_e Z_0 R_0 B_f \omega_e Q}{2a^2 \omega} \left[1 + jQ \left(\frac{\omega_e}{\omega} - \frac{\omega}{\omega_e} \right) \right]^{-1} \quad (6)$$

where the resonance is at the electron bounce frequency $\omega_e \approx c\sqrt{2\pi r_e n_p}$, n_p is the volume density of the proton beam, and ω_e/Q is the spread in ω_e due to lattice variation. All internal surfaces including ferrite are coated with TiN to suppress electron multipacting. The 100 nm thickness is expected to sustain proton-halo bombardment without eddy-current heating. Injection stripped electrons are guided to the collectors with a low backscattering yield. A voltage up to ± 1 kV can be applied to 42 BPMs, together with a dedicated electrode in the injection region, to clear electrons and to isolate areas of high electron concentration. A beam-in-gap kicker ensures a clean beam-gap. Vacuum ports can be screened, and steps in the vacuum pipe are tapered to reduce peaked electric fields causing electron emission. A vacuum pressure of 10^{-8} Torr minimizes gas ionization. Solenoids can be wound in straight sections to reduce multipacting [5].

2.4 Other sources

Space-charge force is represented by reactive impedances

$$Z_{\parallel}^{sc} = -j \frac{n g_0 Z_0}{2\beta \gamma^2}; \quad Z_{\perp}^{sc} = -j \frac{R_0 Z_0}{\beta^2 \gamma^2} \left(\frac{1}{a^2} - \frac{1}{b^2} \right) \quad (7)$$

Longitudinally, the debunching force (below γ_T) raises the stability threshold by 4 times [9]. Transversely, it causes frequency shift and lowers the stability threshold, when the low-frequency part is damped by the chromaticity [10].

The lengths L_{BPM} of stripline BPMs are chosen to be 0.25 m so that the lowest resonance frequency $c/4L_{BPM} \approx 300$ MHz is much higher than the bunch characteristic frequency $\beta c/2\pi R_0 B_f \approx 2.4$ MHz.

The steps in vacuum pipe are designed with the tapering length at least three times longer than the step height to avoid sharp discontinuities and resonances. Vacuum ports

and valves are shielded to reduce the coupling. On the other hand, bellows, many housed inside correctors, are not shielded to avoid mechanical complications. All these contribute to broad-band reactive impedance small in comparison with that of space charge and extraction kickers [11].

RF cavities are bench-measured to determine the parasitic impedance. The dominant parasitic modes are in 7 - 10 MHz range, due to standing waves on the bus-bars connecting the two accelerating gaps. The cavity shroud contains sufficient room for resistive glow bars to damp (de-Q) the resonances.

3 DAMPING ENHANCEMENT

H^- charge-exchange injection facilitates transverse phase-space painting to reduce space-charge effects [1]. Energy correctors and spreaders in the pre-injection transport facilitate longitudinal painting to enhance Landau damping without extending momentum halo [12]. A dual-harmonic RF system enhances the bunching factor by about 20% and reduces the peak space-charge tune spread accordingly. A four-family sextupole correction ensures adequate momentum acceptance (more than $\pm 1\%$).

A fast, wide-band feedback system can be implemented to damp instabilities. Three frequency ranges are of interest: 0.2-0.8 MHz (depending on operating point) with growth rates of about 5 ms^{-1} due to the resistive-wall impedance exciting the lowest betatron sideband; 5-30 MHz with growth rates of about 10 ms^{-1} due to the extraction-kicker impedance; and 100-200 MHz with growth rates of 30-100 ms^{-1} due to e-p instability. The stripline kicker designed for beam-in-gap cleaning can be used as a damping kicker. Additional space is also reserved for future implementations.

4 SUMMARY

This paper summarizes design implementations in the SNS ring to control collective effects including space charge, transverse and longitudinal instabilities, and electron cloud. Efforts are made to minimize leading sources of beam-coupling impedances, and to enhance Landau damping. With the design baseline, up to 1.4 MW (1.5×10^{14} protons per pulse) beam power can be stored without encountering instability and excessive beam loss.

We thank A. Aleksandrov, I. Hofmann, H. Ludewig, W. Meng, J. Mi, J. Sandberg, N. Simos, N. Tsoupas, J. Tuozolo, B. Zotter for many discussions.

5 REFERENCES

- [1] J. Wei et al, Phys. Rev. ST-AB, **3** (1999) 080101
- [2] A. Fedotov, I. Hofmann, Phys. Rev. ST-AB, **5** (2002) 024202
- [3] J. Herrera, B. Zotter, BNL-TID4500 (1978)
- [4] N. Tsoupas et al, EPAC (2000) 1581
- [5] J. Wei, R. Macek, ECLLOUD'02, CERN-2002-001
- [6] D. Davino et al, BNL/SNS/102 (2001); these proceedings
- [7] A. Piwinski, PAC77 1364; V. Danilov et al, these proceedings
- [8] K. Ohmi et al PRL, **85** (2000) 3821; PRE, **65** (2002) 16502
- [9] K. Woody et al, PAC (2001) 2057
- [10] A. Fedotov et al, these proceedings
- [11] S.Y. Zhang, BNL/SNS/61 (1999)
- [12] D. Raparia, et al, HB2002, FNAL (2002)